Received September 1999
Revised July 2000
Accepted July 2000

The volume of fluid method in spherical coordinates

A.M.C. Janse, P.E. Dijk and J.A.M. Kuipers
Department of Chemical Technology, Twente University, Enschede, The Netherlands

Keywords *Numerical methods, Fluids, Flow, Patterns*

Abstract *The volume of fluid (VOF) method is a numerical technique to track the developing free surfaces of liquids in motion. This method can, for example, be applied to compute the liquid flow patterns in a rotating cone reactor. For this application a spherical coordinate system is most suited. The novel derivation of the extended VOF algorithms for this class of applications is presented here. Some practical limitations of this method, that are inherent in the geometry of the described system, are discussed.*

Nomenclature

A = acceptor cell
d = distance (m)
d′ = distance between the surface of a cell and the boundary in the direction of the interpolation cell (m)
D = donor cell
E = empty cell
F = fraction of volume (–)
F = full liquid cell
i = discrete r-coordinate index (–)
j = discrete θ-coordinate index (–)
n = discrete time coordinate index (–)
P = dimensionless pressure defined by equation (37) (–)
r = radial spherical coordinate (m)
S = surface cell
t = time coordinate (s)
v = velocity (m/s)
V = volume (m^3)

Greek symbols
Δ = distance, interval
δ = dimensionless film coordinate defined by equation (38) (–)
θ = angular spherical coordinate (rad)
ν = kinematic viscosity (m/s)
φ = rotational spherical coordinate (rad)
ω = angular velocity (rad/s)

Other symbols
∇ = divergence (–)

Sub- and superscripts
a = adjacent, atmospheric
c = cell center
film = film
i = inflow
I = interpolation cell
o = outflow
up = upflow
w = wall

1. Introduction

Conventional finite difference representations of fluid flow equations (i.e. Navier-Stokes equations) often introduce averaging of the hydrodynamic key variables. This averaging results in a smoothing of spatial variations in flow variables and in particular in a smearing of discontinuities as encountered in the vicinity of a free surface. In order to apply the free surface boundary conditions to the discretized conservation equations and to advect the fluid through the computational mesh without any smearing of the free surface, the location of the free surface has to be determined. Conventional discrete Eulerian

International Journal of Numerical Methods for Heat & Fluid Flow, Vol. 10 No. 7, 2000, pp. 654-674.

This investigation was supported by the CEC-AIR program (AIR-contract CT93-0889).

convective flow computations require an averaging of the flow variables of all fluid elements flowing through a grid cell during some time interval. This averaging process results in a smoothing of all variations in flow variables and in particular in a smearing of the free surface discontinuities. For this purpose, several numerical methods have been developed in the past. Hirt and Nichols (1981) and Rudman (1997) presented overviews of these computational methods. Hirt and Nichols (1981) briefly discussed the technique of height and line functions, the marker and cell (MAC) method and the simplified version of this technique (SMAC). However, these techniques all possess certain drawbacks which limit their range of applicability. For instance, the height function technique is not able to describe flows with complex interface topology and three-dimensional surfaces, whereas the implementation of the method of line functions is very difficult in the case of intersecting surfaces. The MAC and even the SMAC method require large computer memories and a substantial amount of CPU resources. Therefore, Hirt and Nichols (1981) proposed a completely new computational technique for free surface flows termed the volume of fluid (VOF) method. Rudman (1997) compared four different surface tracking methods, i.e. simplified line interface calculation (SLIC) (Noh and Woodward, 1976), Hirt-Nichols' VOF (Hirt and Nichols, 1981), flux-corrected transport volume of fluid (FCT-VOF) (Rudman, 1997) and Youngs' VOF (Youngs, 1982). He tested these methods using the two-dimensional advection of hollow squares and a hollow circle in unidirectional velocity fields, the rotation of a slotted circle, the shearing flow of a circle, and a Rayleigh-Taylor instability. He concludes that the applicability of a surface tracking method depends strongly on the system under investigation. In general, more complex schemes (e.g. FCT-VOF and Youngs' VOF) are much more difficult to implement, but yield more accurate results. Hirt and Nichols-VOF will be outlined below, together with practical limitations, in relation to the description of liquid films flowing along the conical surface of a rotating cone reactor. Results obtained with our numerical model in which the VOF-technique has been incorporated are presented elsewhere (Janse *et al.*, forthcoming). In this work it will be assumed that the liquid flow in the rotating cone is symmetrical in the direction of rotation. Therefore, all quantities describing the flow are independent of the ϕ-coordinate (and only dependent on the r- and/or θ-coordinate (see Figure 1)).

2. Construction of the free surface

An important aspect of the VOF-methodology is the introduction of a characteristic marker quantity, called the fractional amount of fluid (F) with which the fluid from the void can be distinguished. This marker quantity is defined as follows:

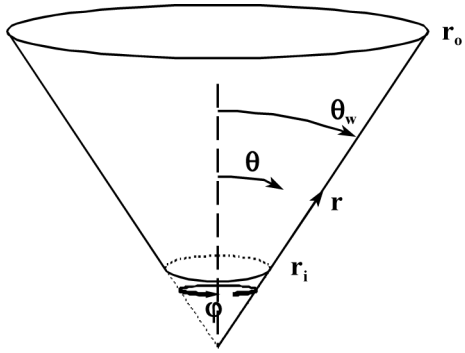

Figure 1.
Applied spherical coordinate system

$$F = \begin{cases} 1 & \text{fluid} \\ 0 & \text{void} \end{cases} \tag{1}$$

The location of the free surface is defined by the discontinuity in the fraction of volume, as indicated in Figure 2.

According to the VOF-approach, the free surface is represented as a set of discrete discontinuous line segments. The free surface in each free surface cell is constructed either oriented parallel or perpendicular to the r-coordinate.

The main orientation of the free surface line segments depends on the gradient of F in the cells adjacent to the cells containing the free surface. To identify these cells, empty, internal fluid and free surface cells are defined. An empty cell is defined as a cell with a zero F-value:

$$F_{i,j} = 0 \tag{2}$$

where i and j represent the index of the discrete cells (or grid points) in the r- and θ-direction, respectively, of the computational domain. An internal fluid cell is defined as a cell which is not empty and has no adjacent empty cells

$$0 < F_{i,j} \leq 1 \wedge \left(F_{i+1,j} \neq 0 \wedge F_{i-1,j} \neq 0 \wedge F_{i,j+1} \neq 0 \wedge F_{i,j-1} \neq 0\right) \tag{3}$$

whereas a surface cell is defined as a cell which is not empty and has at least one adjacent empty cell

$$0 < F_{i,j} \leq 1 \wedge \left(F_{i+1,j} = 0 \vee F_{i-1,j} = 0 \vee F_{i,j+1} = 0 \vee F_{i,j-1} = 0\right) \tag{4}$$

To determine the mean orientation of the free surface within a free surface cell, it is assumed that the free surface can be approximated by a straight line

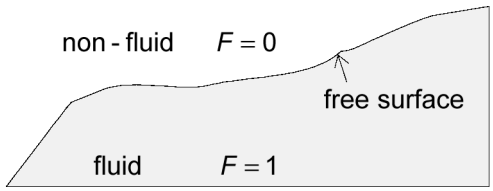

Figure 2.
Volume of fluid method for free surfaces: fraction of volume

separating the fluid from the void. If the magnitude of the calculated slope of the line indicates that the line is oriented to a larger extent along the r-coordinate, the line is assumed to be parallel to the r-coordinate. Otherwise, the line is assumed to be perpendicular to the r-coordinate. The free surface can thus be represented either as a single valued function $\Theta(r)$ or as a single valued function $R(\theta)$, depending on the magnitude of the slope. The slope of the free surface represented as $\Theta(r)$ is approximated by:

$$\left(\frac{d\Theta}{dr}\right)_i^n = \frac{\Theta_{i+1}^n - \Theta_{i-1}^n}{2\Delta r} \tag{5}$$

where $\Theta(r)$ is approximated as follows:

$$\Theta^n(r_i)\big|_{j=j-\frac{3}{2}} = 0 \wedge \Theta^n(r_i) = \Theta_i^n = \left(F_{i,j-1}^n + F_{i,j}^n + F_{i,j+1}^n\right)\Delta\theta \tag{6}$$

A similar calculation is performed for $R(\theta)$ in which the slope is approximated by:

$$\left(\frac{dR}{d\theta}\right)_j^n = \frac{R_{j+1}^n - R_{j-1}^n}{2\Delta\theta} \tag{7}$$

where $R(\theta)$ is approximated as:

$$R^n(\theta_j)\big|_{i=i-\frac{3}{2}} = 0 \wedge R^n(\theta_j) = R_j^n = \left(F_{i-1,j}^n + F_{i,j}^n + F_{i+1,j}^n\right)\Delta r \tag{8}$$

The normalized derivative with the smallest magnitude is considered to provide the best approximation of the slope, because the corresponding $\Theta(r)$ or $R(\theta)$ approximation is more accurate in that case. If the slope is best described by $\Theta(r)$ in which

$$\left|\frac{1}{r_i}\left(\frac{dR}{d\theta}\right)_j^n\right| > \left|r_i\left(\frac{d\Theta}{dr}\right)_i^n\right| \tag{9}$$

the free surface is oriented along the r-coordinate and is assumed to be parallel to the r-coordinate. Otherwise the free surface is assumed to be perpendicular to the r-coordinate. This procedure to approximate the actual free surface orientation is depicted in Figure 3 for a slope described by $R(\theta)$.

3. Free surface advection

The equation describing the propagation of the free surface is given by the following transport equation for F:

$$\left.\frac{DF}{Dt}\right|_{i,j}^{n+1} = \left.\frac{\partial F}{\partial t}\right|_{i,j}^{n+1} + (\nabla \cdot Fv)_{i,j,\partial r}^{n+1} + (\nabla \cdot Fv)_{i,j,\partial\theta}^{n+1} + (\nabla \cdot Fv)_{i,j,\partial\phi}^{n+1} = 0 \tag{10}$$

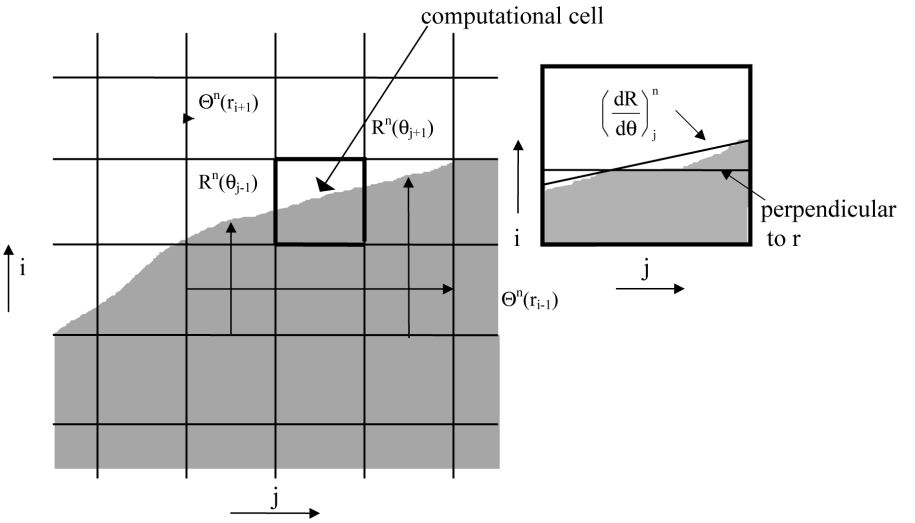

Figure 3.
Approximation of actual free surface orientation for a slope described by $R(\theta)$

This equation is discretized by integration over the mass conservation control volume, which coincides with the Eulerian grid cells; its boundaries are the Eulerian grid cell boundaries. The equation is discretized at the advanced time level n + 1 using explicit finite difference representations of the convective terms. Since the computation of the fraction of volume values constitutes the last step of the flow field computations, the velocity field for the advanced time level is already available in evaluating these terms.

The solution of the fraction of volume equation is performed sequentially by applying two sweeps through the mesh to account for the convective transport in each of the r- and θ-direction. The reason for the application of this sequential technique is the rather complex advection method that has to be applied to avoid excessive computational smearing of the interface.

The first order derivative of the accumulation term appearing in equation (10) is approximated by a first order backward finite difference representation:

$$\left.\frac{\partial F}{\partial t}\right|^{n+1}_{i,j} = \frac{F^{n+1}_{i,j} - F^{n}_{i,j}}{\Delta t} \tag{11}$$

The convective fluxes are approximated by the donor-acceptor finite differencing scheme which takes the orientation of the reconstructed free surface into account. For the convective transport between two internal fluid cells, this scheme reduces to the well-known upwind discretization scheme. The resulting finite difference representation of the convective terms for internal fluid cells is presented below. Although it is in principle not necessary to compute the fraction of volume flow between two internal fluid cells, this computation is applied due to the one-dimensional nature of the presented technique. Owing to the assumption of symmetry of the flow field in the direction of rotation (φ-direction), the last term in the left-hand side of equation

(10) is neglected. The resulting discrete convection terms for internal fluid cells are presented below:

$$(\Delta\cdot \mathrm{Fv})^{n+1}_{i,j,\partial r} = \frac{1}{r_i^2}\frac{\left\langle r^2_{i+\frac{1}{2}}\, F^{n+1}_{i+\frac{1}{2},j}\, v^{n}_{r,i+\frac{1}{2},j}\right\rangle - \left\langle r^2_{i-\frac{1}{2}}\, F^{n+1}_{i-\frac{1}{2},j}\, v^{n}_{r,i-\frac{1}{2},j}\right\rangle}{\Delta r} \tag{12}$$

$$(\Delta\cdot \mathrm{Fv})^{n+1}_{i,j,\partial\theta} = \frac{1}{r_i \sin\theta_j}\frac{\left\langle \sin\theta_{j+\frac{1}{2}}\, F^{n+1}_{i,j+\frac{1}{2}}\, v^{n}_{\theta,i,j+\frac{1}{2}}\right\rangle - \left\langle \sin\theta_{j-\frac{1}{2}}\, F^{n+1}_{i,j-\frac{1}{2}}\, v^{n}_{\theta,i,j-\frac{1}{2}}\right\rangle}{\Delta\theta} \tag{13}$$

$$(\Delta\cdot \mathrm{Fv})^{n+1}_{i,j,\partial\phi} = 0 \tag{14}$$

with:

$$\left\langle r^2_{i+\frac{1}{2}}\, F^{n+1}_{i+\frac{1}{2},j}\, v^{n}_{r,i+\frac{1}{2},j}\right\rangle = \begin{cases} r^2_{i+\frac{1}{2}}\, F^{n+1}_{i+1,j} v^{n}_{r,i+\frac{1}{2},j} & \text{if} \quad v^{n}_{r,i+\frac{1}{2},j} \le 0 \\ r^2_{i+\frac{1}{2}}\, F^{n+1}_{i,j} v^{n}_{r,i+\frac{1}{2},j} & \text{if} \quad v^{n}_{r,i+\frac{1}{2},j} > 0 \end{cases} \tag{15}$$

$$\left\langle \sin\theta_{j+\frac{1}{2}}\, F^{n+1}_{i,j+\frac{1}{2}}\, v^{n}_{\theta,i,j+\frac{1}{2}}\right\rangle = \begin{cases} \sin\theta_{j+\frac{1}{2}}\, F^{n+1}_{i,j+1} v^{n}_{\theta,i,j+\frac{1}{2}} & \text{if} \quad v^{n}_{\theta,i,j+\frac{1}{2}} \le 0 \\ \sin\theta_{j+\frac{1}{2}}\, F^{n+1}_{i,j} v^{n}_{\theta,i,j+\frac{1}{2}} & \text{if} \quad v^{n}_{\theta,i,j+\frac{1}{2}} > 0 \end{cases} \tag{16}$$

Owing to the aforementioned fully explicit nature of the discretised free surface advection equation, only small changes in the fraction of volume values per time level are allowed. Therefore, the time step for the solution of the F-equation must be small compared to the time step used for the simultaneous solution of the mass and momentum conservation equations using a semi-explicit technique. This is implemented by dividing the time step Δt used for the solution of the mass and momentum conservation equations into $\hat{n}_{max}$ smaller time intervals of magnitude $\Delta t'$:

$$\Delta t' = \frac{\Delta t}{\hat{n}_{max}} \wedge \hat{n}_{max} >> 1 \tag{17}$$

and computing the fraction of volume equation for each of these time sub-intervals. Typically a value of 25 was used for $\hat{n}_{max}$.

The convective contributions through the grid cell faces between two cells, of which at least one is a free surface cell, are computed using the donor-acceptor (DA) finite difference approximation. The DA approximation distinguishes the donor cell D, donating the mass or volume, from the acceptor

cell A, accepting this mass or volume. The associated transport depends on the sign of the grid cell face velocity. Additionally, the upstream cell of the donor cell D_{up} is identified.

The DA differencing technique will be explained for the fraction of volume advection through the grid cell face (i + ½, j) between a cell (i, j) and its adjacent cell (i + 1, j). The computations for all other cell faces are analogous to this approach.

This DA identification scheme of the computational cells is written as follows:

$$D_{up} = \begin{cases} (i+2,j) \\ (i-1,j) \end{cases} \wedge D = \begin{cases} (i+1,j) \\ (i,j) \end{cases} \wedge A = \begin{cases} (i,j) & \text{if } v_{r,i+\frac{1}{2},j}^{n} \leq 0 \\ (i+1,j) & \text{if } v_{r,i+\frac{1}{2},j}^{n} > 0 \end{cases} \tag{18}$$

It is necessary to determine whether the acceptor or the donor cell is to be used to determine the F-value required to evaluate the convective transport term. This choice depends on the free surface orientation, the acceptor cell type and the cell type located upstream of the donor cell. The acceptor cell is used when the surface is advected normal to itself. In case of advection parallel to the surface, the donor cell is used. However, if the acceptor cell or the cell upstream of the donor cell is empty, the acceptor cell is used regardless of the mean free surface orientation. This procedure is expressed as follows:

$$AD = \begin{cases} A \text{ if } & \left| \frac{1}{r_i} \left(\frac{dR}{d\theta} \right)_j^{\hat{n}} \right| \leq \left| r_i \left(\frac{d\Theta}{dr} \right)_i^{\hat{n}} \right| \vee F_A^{\hat{n}} = 0 \vee F_{D_{up}}^{\hat{n}} = 0 \\ D \text{ if } & \left| \frac{1}{r_i} \left(\frac{dR}{d\theta} \right)_j^{\hat{n}} \right| > \left| r_i \left(\frac{d\Theta}{dr} \right)_i^{\hat{n}} \right| \wedge 0 < F_A^{\hat{n}} \leq 1 \wedge 0 < F_{D_{up}}^{\hat{n}} \leq 1 \end{cases} \tag{19}$$

in which $\hat{n}$ refers to the time level of the volume of fluid calculation.

The volume of the donor cell is given by:

$$V_D = 2\pi r_D^2 \sin\theta_j \Delta r \Delta\theta \tag{20}$$

which is used to compute the maximum amount of fluid and void that can be transported through the grid cell face during a certain time level.

The fractional amount of fluid crossing a cell face in the radial direction at grid index (i + ½, j) is given by:

$$\Delta V_D = 2\pi r_{i+\frac{1}{2}}^2 \sin\theta_j \left| v_{r,i+\frac{1}{2},j}^{n+1} \Delta t' \right| \Delta\theta \tag{21}$$

while in the direction perpendicular to the cone wall ΔV_D at grid index (i, j + ½) is given by:

$$\Delta V_D = 2\pi r_i^2 \sin\theta_{j+\frac{1}{2}} \Delta r \frac{\left| v^{n+1}_{\theta,i,j+\frac{1}{2}} \Delta t' \right|}{r_i} \tag{22}$$

This evaluation is based on the average location of the volume between the previous time level n and the advanced time level n + 1. This is in contrast to Hirt and Nichols (1981) who suggested to employ the location of the volume at the previous time level n, which leads to a poor approximation in the spherical coordinate system used here.

If more fluid should flow from the donor cell than it contains, this flow is reduced in such a manner that at most all the fluid is drawn from the donor cell. Similarly, if more void should flow from the donor cell than it contains, an additional amount of fluid is drawn from the donor cell. These corrections are represented by

$$CF^{\hat{n}+1}_{i+\frac{1}{2},j} = \max\left(\left(1 - F^{\hat{n}}_{AD}\right)\Delta V_D - \left(1 - F^{\hat{n}}_{D}\right)V_D, 0\right) \tag{23}$$

The fractional amount of fluid which is actually transported during the time interval is given by:

$$\Delta(FV)^{\hat{n}+1}_{i+\frac{1}{2},j} = \min\left(F^{\hat{n}}_{AD}\Delta V_D + CF^{\hat{n}+1}_{i+\frac{1}{2},j}, F^{\hat{n}}_{D} V_D\right) \tag{24}$$

from which the corresponding change in F can be obtained:

$$F^{\hat{n}+1}_{D} \leftarrow F^{\hat{n}+1}_{D} - \frac{\Delta(FV)^{\hat{n}+1}_{i+\frac{1}{2},j}}{V_D} \wedge F^{\hat{n}+1}_{A} \leftarrow F^{\hat{n}+1}_{A} + \frac{\Delta(FV)^{\hat{n}+1}_{i+\frac{1}{2},j}}{V_A} \tag{25}$$

As mentioned before, the transport through the other grid cell faces is treated in the same way. Some characteristic examples of the free surface advection through a grid cell face are depicted in Figure 4.

4. Free surface boundary conditions

At the free surface, boundary conditions for the velocities and the pressure have to be enforced. The free surface pressure condition for a surface cell, that is, the pressure of the free surface cell, is obtained by linear interpolation of the known pressure at the free surface location and the pressure of an adjacent internal fluid cell. The free surface velocity values depend on the applied boundary conditions and on the free surface orientation.

The free surface pressure condition for free surface cells is computed via linear interpolation of the pressure at the free surface p_a and the pressure of the nearest internal fluid cell, called the interpolation cell, $p^{n+1}_{I_{i,j}}$, at distances of respectively $d^n_{i,j}$ and 0 from the centre of the interpolation cell:

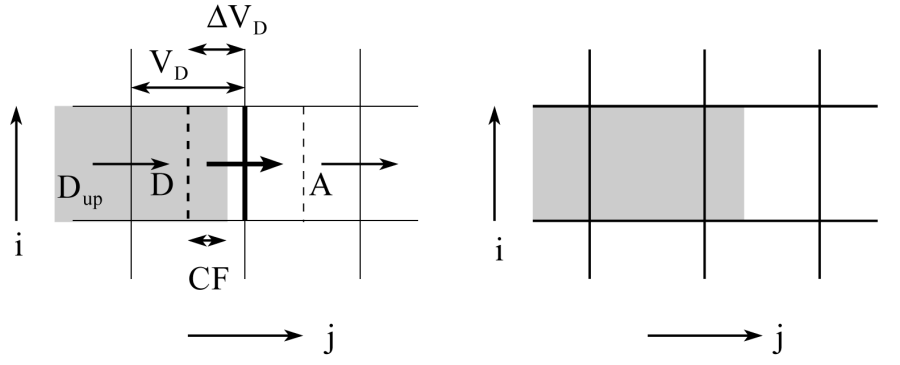

$$AD=D,\ CF=0,\ \Delta(FV)^{n+1}_{i+\frac{1}{2},\,j}=F_D\Delta V_D$$

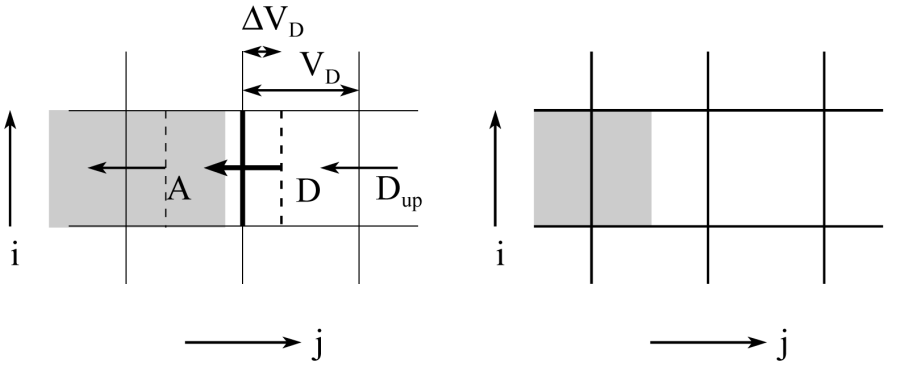

$$AD=A,\ \Delta(FV)^{n+1}_{i+\frac{1}{2},\,j}=CF$$

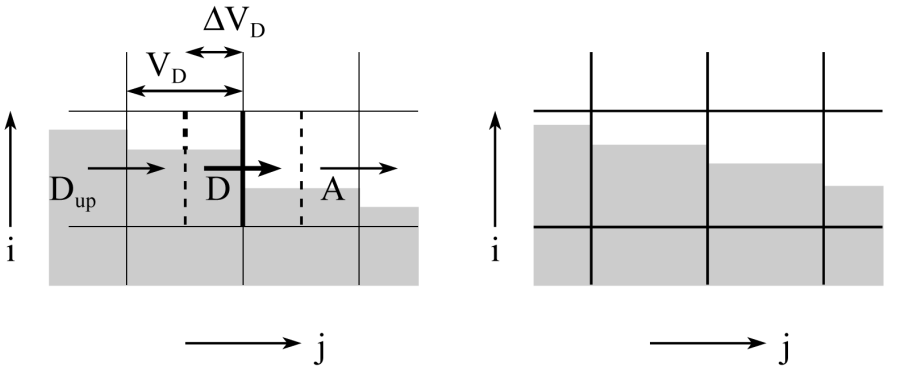

$$AD=A,\ \Delta(FV)^{n+1}_{i+\frac{1}{2},\,j}=CF=0$$

Figure 4.
Three characteristic free surface advection examples through a grid cell face. The dashed lines indicate the vertical boundaries of the control volume for the new time level. $CF^{n+1}_{i+\frac{1}{2},j}$ is abbreviated with CF

$$p = \begin{cases} p_a & \text{if} \quad d = d^n_{i,j} \\ p^{n+1}_{I_{i,j}} & \text{if} \quad d = 0 \end{cases} \tag{26}$$

Linear interpolation yields the pressure of the free surface cell $p^{n+1}_{i,j}$ at a distance from the interpolation cell:

$$p^{n+1}_{i,j} = \left(1 - \frac{d_{i,j,c}}{d^n_{i,j}}\right) p^{n+1}_{I_{i,j}} + \frac{d^n_{i,j,c}}{d^n_{i,j}} p_a \; d = d_{i,j,c} \tag{27}$$

This interpolation procedure is depicted in Figure 5.

In a spherical coordinate system, the algebraic equations for the distances from the centre of the interpolation cell depend on the location and the orientation of the reconstructed free surface. The distances shown in Figure 5 can be obtained from the grid geometry and the F-value of the relevant free surface cell for which the boundary condition has to be set. In this connection also the orientation of the free surface has to be accounted for.

When the surface is oriented in a horizontal direction, the interpolation cell can be located below or above the surface cell, while in case of a vertical orientation, the interpolation cell can be located at the left or the right side of the surface cell. The equations required for the computation of the distances in the pressure interpolation procedure are presented below for these four situations.

Horizontal surface orientation

$$\left| \frac{1}{r_i} \left(\frac{dR}{d\theta} \right)^{n+1}_{j} \right| \leq \left| r_i \left(\frac{d\Theta}{dr} \right)^{n+1}_{i} \right|$$

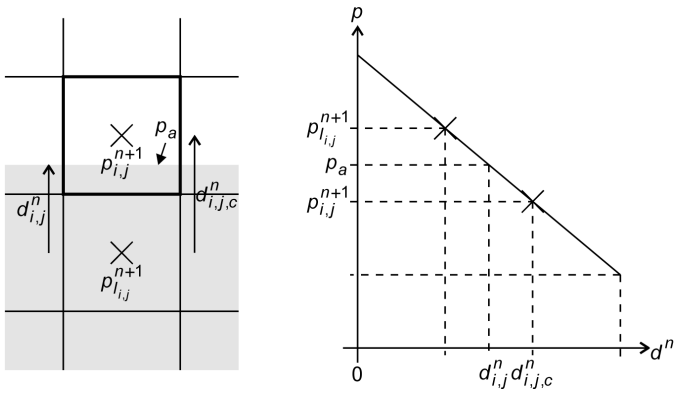

Figure 5.
Free surface cell pressure interpolation

Case 1: interpolation cell below the surface cell:

$$I_{i,j}^{n+1} = (i-1,j) \wedge \frac{d_{i,j,c}^{n+1}}{d_{i,j}^{n+1}} = \frac{1}{\frac{1}{2} + F_{i,j}^{n+1} \frac{r_i^2}{r^2}_{i-\frac{1}{2}}} \quad r_i \left(\frac{d}{dr}\right)_i^{n+1} \leq 0 \tag{28}$$

Case 2: interpolation cell above the surface cell:

$$I_{i,j}^{n+1} = (i+1,j) \wedge \frac{d_{i,j,c}^{n+1}}{d_{i,j}^{n+1}} = \frac{1}{\frac{3}{2} - \left(1 - F_{i,j}^{n+1}\right) \frac{r_i^2}{r^2}_{i-\frac{1}{2}}} \quad r_i \left(\frac{d\Theta}{dr}\right)_i^{n+1} > 0 \tag{29}$$

Vertical surface orientation

$$\left| \frac{1}{r_i} \left(\frac{dR}{d\theta}\right)_j^{n+1} \right| > \left| r_i \left(\frac{d\Theta}{dr}\right)_i^{n+1} \right|$$

Case 1: interpolation cell at the left side of the surface cell

$$I_{i,j}^{n+1} = (i,j-1) \wedge \frac{d_{i,j,c}^{n+1}}{d_{i,j}^{n+1}} = \frac{r_i \Delta\theta}{\frac{1}{2} r_i \Delta\theta + d_{i,j}'^{n+1}} \quad \frac{1}{r_i} \left(\frac{dR}{d\theta}\right)_j^{n+1} \leq 0 \tag{30}$$

with

$$\frac{r_i \Delta\theta}{\frac{1}{2} r_i \Delta\theta + d_{i,j}' n + 1} \approx$$

$$\begin{cases} \dfrac{1}{\frac{1}{2} - \dfrac{\theta_{j-\frac{1}{2}}}{\Delta\theta} + \sqrt{\left(\dfrac{\theta_{j-\frac{1}{2}}}{\Delta\theta}\right)^2 + \dfrac{2F_{i,j}^{n+1} \sin\theta_j}{\Delta\theta}}} & \text{if} \quad \theta_{j-\frac{1}{2}} \approx 0 \ \wedge \ d_{i,j}'^{\,n+1} << r_i \\ \dfrac{1}{\frac{1}{2} + F_{i,j}^{n+1} \dfrac{\sin\theta_j}{\sin\theta_{j-\frac{1}{2}}}} & \text{if} \quad \theta_{j-\frac{1}{2}} >> \frac{1}{2} \dfrac{d_{i,j}^{n+1}}{r_i} \end{cases} \tag{31a,b}$$

while d′ stands for the distance between the surface inside the cell and the cell boundary in the direction of the interpolation cell.

Case 2: interpolation cell at the right side of the surface cell:

$$I_{i,j}^{n+1} = (i,j+1) \wedge \frac{d_{i,j,c}^{n+1}}{d_{i,j}^{n+1}} = \frac{r_i \Delta\theta}{\frac{3}{2} r_i \Delta\theta - d_{i,j}'^{n+1}} \quad \frac{1}{r_i} \left(\frac{dR}{d\theta}\right)_j^{n+1} > 0 \tag{32}$$

In case:

$$\theta_{j-\frac{1}{2}} >> \frac{1}{2}\frac{d'^{n+1}_{i,j}}{r_i} \tag{33}$$

equation (32) can be written as follows:

$$\Rightarrow \frac{d^{n+1}_{i,j,c}}{d^{n+1}_{i,j}} = \frac{r_i \Delta\theta}{\frac{3}{2} r_i \Delta\theta - d'^{n+1}_{i,j}} \approx \frac{1}{\frac{3}{2} - \frac{\left(1-F^{n+1}_{i,j}\right)\sin\theta_j}{\sin\theta_{j-\frac{1}{2}}}} \tag{34}$$

The pressure of a free surface cell and the pressure of its adjacent internal fluid cell are coupled by the free surface pressure equation. Therefore, the free surface pressure equation cannot be solved directly, but must be computed together with the pressures obtained from the solution of the Pressure Poisson Equation (PPE).

The free surface pressure condition implies the presence of an interpolation cell. Problems arise when a partially filled free surface cell lies adjacent to a fictitious prescribed pressure boundary cell, with a free surface boundary parallel to the physical boundary. In this case, the pressure of the free surface cell is virtually linked to itself and uncouples from all other cells, resulting in an undefined pressure for both cells. To overcome this problem, the orientation of the free surface boundary is treated as if it were perpendicular to the physical boundary, instead of parallel. This undesired situation can occur, for example, when the fluid layer is captured in only one grid cell in the θ-direction. In that case, the influence of the no-slip boundary condition is relatively large on the calculated r-velocity distribution in θ-direction. Moreover, to fulfil continuity, the velocity at the surface of the layer (which is the only other r-velocity which is calculated at constant radial coordinate) will be overestimated to a large extent to compensate for the no-slip boundary condition at the wall. This situation of extremely steep r-velocity gradients in θ-direction must be avoided by a careful selection of the applied numerical grid layout for each physical situation. The decreasing film thickness with increasing radial coordinate together with an increasing size of the grid cells perpendicular to the cone wall with increasing radial coordinate make this requirement a non-trivial task. As an example, Figure 6 shows the distribution of the film over the grid cells in the θ-direction. Increasing the number of grid cells in the θ-direction leads to exceedingly small grid cell dimensions at lower values of the radial coordinate. Exceedingly small time intervals must be used in the simulations to satisfy the Courant stability condition which lead to extensive calculation times.

The free surface pressure condition is supplemented with the specification of the velocities immediately outside the free surface. These velocities are needed in the finite-difference approximations for points lying just outside the fluid. The velocities between every free surface and empty cell are solved explicitly from the discrete representation of the continuity equation, to conserve the

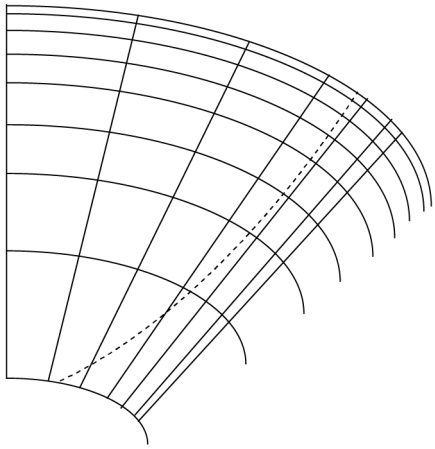

Figure 6.
Distribution of the film over a few grid cells in the θ-direction. The dashed line represents the fluid film

volume flowing through free surface cells. When a free surface cell has a single neighbouring empty cell and thus a single unknown velocity, this velocity is solved from the following equation:

$$\frac{\rho}{r_i^2}\frac{r^2_{i+\frac{1}{2}}v^{\tilde{n}+1}_{r,i+\frac{1}{2},j}-r^2_{i-\frac{1}{2}}v^{\tilde{n}+1}_{r,i-\frac{1}{2},j}}{\Delta r}+\frac{\rho}{r_i\sin\theta_j}\frac{\sin\theta_{j+\frac{1}{2}}v^{\tilde{n}+1}_{\theta,i,j+\frac{1}{2}}-\sin\theta_{j-\frac{1}{2}}v^{\tilde{n}+1}_{\theta,i,j-\frac{1}{2}}}{\Delta\theta}=0 \quad (35)$$

For a free surface cell with two neighbouring empty cells and thus two unknown velocities, they are each solved from the two separate transport terms:

$$\frac{\rho}{r_i^2}\frac{r^2_{i+\frac{1}{2}}v^{\tilde{n}+1}_{r,i+\frac{1}{2},j}-r^2_{i-\frac{1}{2}}v^{\tilde{n}+1}_{r,i-\frac{1}{2},j}}{\Delta r}=0 \ \wedge \ \frac{\rho}{r_i\sin\theta_j}\frac{\sin\theta_{j+\frac{1}{2}}v^{\tilde{n}+1}_{\theta,i,j+\frac{1}{2}}-\sin\theta_{j-\frac{1}{2}}v^{\tilde{n}+1}_{\theta,i,j-\frac{1}{2}}}{\Delta\theta}=0 \quad (36)$$

When a free surface has three neighbouring empty cells and thus three unknown velocities, the two adjacent velocities are set to zero and the third velocity is solved in the same way a single unknown velocity is solved. These three situations are depicted in Figure 7.

Zero gradient values for the velocities located at free surface boundaries are applied in the following way. The velocity tangential to the free surface cells, located between two empty cells adjacent to the two free surface cells, is set equal to the velocity tangential to the free surface cells, located between the two free surface cells. This is schematically represented in Figure 8.

The whole set of conservation and momentum equations, together with the (initial and) boundary conditions and the solution algorithm is briefly presented in the Appendix.

5. Solutions of remaining problems

The one-dimensional nature of the donor-acceptor algorithm used in our calculations may introduce the effect of void encaptured in internal fluid cells. There are two mechanisms that lead to this phenomenon which is most pronounced when a highly irregular free surface geometry prevails with rapid temporal variation. The first mechanism occurs when void flows from a free surface cell to an adjacent internal fluid cell (see Figure 9) or to an adjacent free surface cell which changes into an internal fluid cell (see Figure 10).

The second mechanism prevails when a free surface has both a parallel and a perpendicular orientation with respect to a coordinate, within a block of four

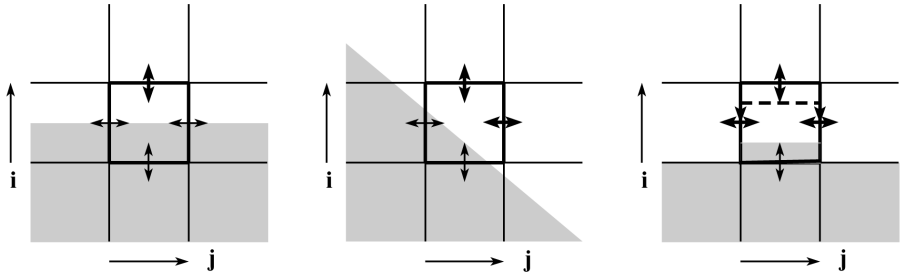

Figure 7. Free surface volume conservation: single (left), two (middle) and three (right) unknown velocities between free surface and empty cells

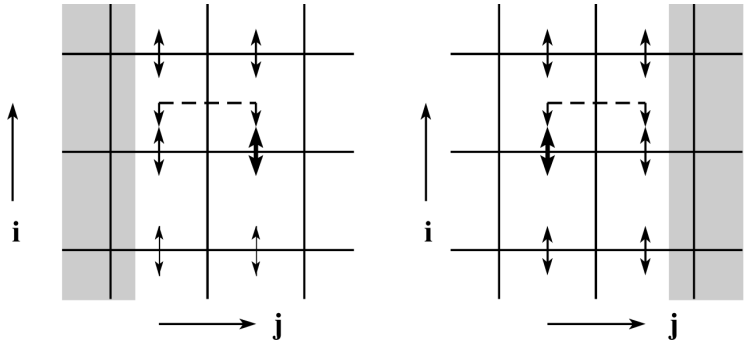

Figure 8. Free surface boundary condition for zero-gradient velocities tangential to and outside of free surface cells

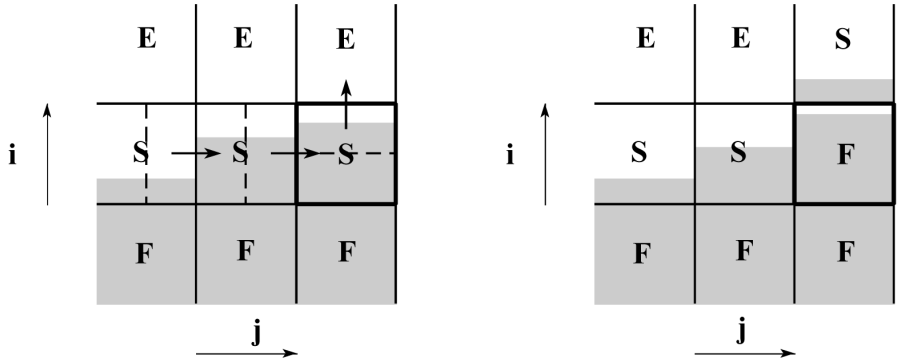

Figure 9. First void encapturing mechanism (F = fluid cell, E = empty cell, S = surface cell). The dashed lines indicate the distance travelled by the surface in a single time step

grid cells. Within this block of grid cells, an empty grid cell adjacent to two free surface cells, one with a parallel and one with a perpendicular free surface orientation, is present. In this situation, one of the free surfaces can propagate through the grid cell boundary between the free surface cell and the empty cell. The other free surface cell thus becomes an internal fluid cell and is treated as such in the algorithm. To avoid this situation as much as possible, small grid cell sizes and small time steps must be applied. In Figure 10 a situation is depicted where both the first and the second mechanism occur simultaneously.

It was found computationally that the encapturing of void can be significantly reduced by employing small grid cell dimensions and small time steps. Furthermore, it is possible that liquid in a grid cell adjacent to the wall reaches the outflow boundary later in time than liquid in a grid cell two cells away from the wall. In this case, actual surface cells will be treated as internal surface cells. To avoid this erroneous treatment, the zero gradient outflow condition is only applied when the liquid is actually flowing out of the cone. Otherwise, boundary cells are treated as empty cells.

As mentioned before in a previous article (Janse *et al.*, forthcoming) clear transitions in the film thickness along the radial coordinate (peaks) are observed at certain locations where the free surface of the film steps from one column in the θ-direction to the next column, as depicted in Figure 11. These jumps are due to an inaccurate approximation of the pressure calculation in the row of cells below the row where the mentioned transition occurs. The result of this inaccurate approximation is an overestimation of the pressure in this row.

There are two main reasons for these high pressures at the row below the row with a column jump:

- The thin fluid layer occupies only a few columns, which has already been discussed (see Figure 6).
- The linear interpolation of the free-surface pressure underestimates the real pressure at the surface.

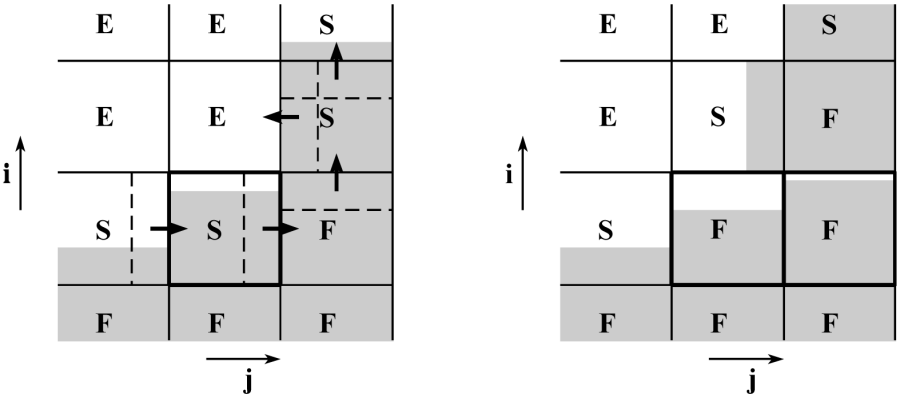

Figure 10.
First and second void encapturing mechanism (F = fluid cell, E = empty cell, S = surface cell). The dashed lines indicate the distance travelled by the surface in a single time step

The pressure profile, as calculated with an approximate analytical solution of the Navier-Stokes equations (see Janse *et al.*, forthcoming) revealed a non-linear profile in the θ-direction. A typical example of such a profile is plotted (indicated with markers) in Figure 12, which shows the dimensionless pressure, defined as:

$$P = \frac{p - p_a}{\rho(\nu\omega)^{1}/_{2}\,\omega r \sin\theta_w} \tag{37}$$

as a function of the dimensionless film coordinate δ, defined as:

$$\delta = d/d_{film} \tag{38}$$

in which d stands for the distance from the wall and d_{film} for the thickness of the film. As is evident from this Figure, a linear interpolation near the surface is allowed because of the linearity of the pressure profile for values of δ close to 1. However, when the fluid layer is only captured in a few columns in the

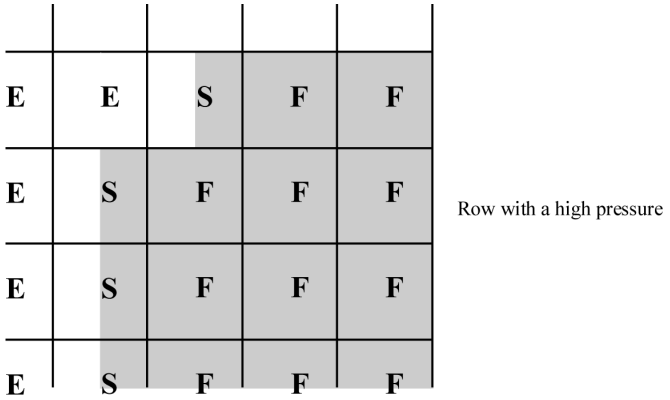

Figure 11.
Transmission point of the free surface (location of the "jump" in thickness) (F = fluid cell, E = empty cell, S = surface cell)

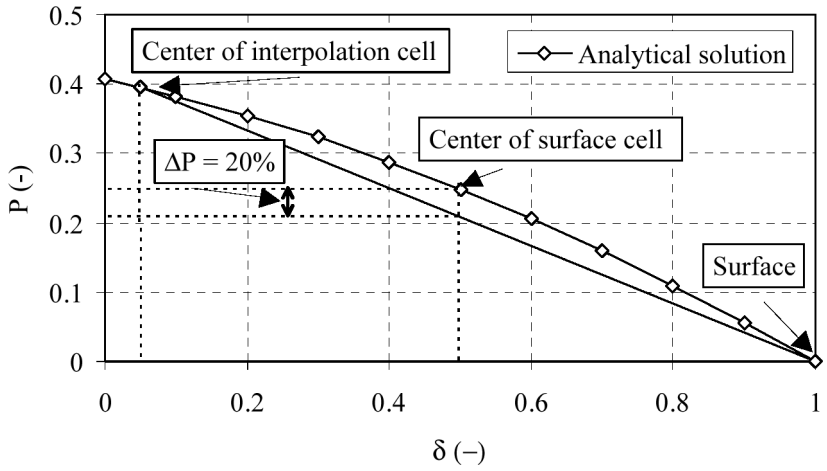

Figure 12.
Graphical presentation of the linear free-surface interpolation. The analytical solution is indicated with markers

θ-direction and the interpolation performed is based on an interpolation cell very close to the wall, this implies a very crude approximation of the curvature of the actual pressure profile. The approximation is influenced further in a negative manner by the application of the variable grid which increases the physical distance between the surface cell and the interpolation cell, although the number of grid cells is not changed. In other words, the centre of the cell from which the interpolation is performed is much closer to the wall than to the free-surface. When the number of grid cells decreases, the inaccuracy of the linear interpolation increases. This can be observed in Figure 12, in which the large physical distance is shown between the centre of the interpolation cell and the surface due to the small number of grid cells (two in θ-direction). In this case, deviations in the pressure calculation between the analytical solution and the numerical approximation can exceed 20 per cent.

The effect of this inaccurate treatment of the pressure boundary condition is more severe at transition points, where the number of grid cells (columns) contained in the grid cells changes. In that case, the fluid cell located exactly at the transition point has two surface cells as neighbouring cells, located above and at the left side (see Figure 11). The surface cell near a transition jump has thus an extra free-surface cell located above it in comparison with other surface cells. The calculated pressure of this extra surface cell is relatively low. In general, the pressure of a cell is dependent on the pressure of its neighbouring cells. Thus, the cell located near a column-jump experiences an additional error due to this extra free-surface cell. Because of a lower value of the pressure in the free-surface cell, a higher pressure *difference* occurs, inducing a driving force for transport of liquid into a direction perpendicular to (away from) the cone wall. This problem cannot be easily circumvented by increasing the number of numerical grid cells in θ-direction, because then also the number of transitions increases. Moreover, increasing the number of grid cells in θ-direction leads, when the physical grid size is not changed, to small grid cell sizes, especially near the inlet point of fluid. Because of the Courant stability condition, which states that the fluid may not pass through one grid cell in a time interval, very small time intervals must be chosen. Therefore, the number of transitions has been limited in the simulations (see Janse *et al.*, forthcoming) to decrease the severity of this problem at the expense of the accuracy of the computed solution (order of magnitude of the deviations can be 20 per cent relative to the analytical solution).

6. Conclusions

The mathematical formulation of the extended VOF technique in a spherical coordinate system was derived. This technique can, for example, be applied to compute the free surface of a liquid flowing inside a rotating cone reactor. The thin liquid layers at the top of the rotating cone are shown to interfere with the minimum spatial resolution of the numerical grid at the bottom of the cone. This practical limitation of the presented VOF method is inherent in the geometry of the described system.

References

Bird, R.B., Stewart, W.E. and Lightfoot, E.N. (1960), *Transport Phenomena*, John Wiley & Sons, Inc., New York, NY.

Hirt, C.W. and Nichols, B.D. (1981), "Volume of fluid (VOF) method for the dynamics of free boundaries", *J. Comp. Phys.*, Vol. 39, p. 201.

Janse, A.M.C., Breuer, A.M.M.H.B., Dijk, P.E., Kuipers, J.A.M., Prins, W. and van Swaaij, W.P.M. (forthcoming), "Hydrodynamics of flowing films in the rotating cone reactor, Part I: numerical model and scaling rules".

Kuipers, J.A.M., van Duin, K.J., van Beckum, F.P.H. and van Swaaij, W.P.M. (1992), "A numerical model of gas-fluidized beds", *Chem. Eng. Sci.*, Vol. 47.

Noh, W.F. and Woodward, P. (1976), "SLIC (simple line interface calculation)", in van Dooren, A.I. and Zandbergen, P.J. (Eds), *Lecture Notes in Physics*, Vol. 59, Springer, New York, NY, pp. 330-40.

Rudman, M. (1997), "Volume-tracking methods for interfacial flow calculations", *Int. J. Num. Methods Fluids*, Vol. 24, p. 671.

Youngs, D.L. (1982), "Time dependent multi-material flow with large fluid distortion", in Morton, K.W. and Baines, M.J. (Eds), *Numerical Methods for Fluid Dynamics*, Academic Press, New York, NY, p. 273.

Appendix. Simplified conservation equations in spherical coordinates and computational scheme

The liquid flow prevailing in a rotating cone is governed on a microscopic scale by a set of mass and momentum conservation equations. These equations are derived from the general conservation equation applied to mass and momentum transport and simplified by making suitable approximations. The conservation equations are supplemented with initial and boundary conditions. A complication which arises here is the fact that the free-surface location and associated boundary condition enforcement has to be dealt with.

Model assumptions

First of all, assumptions are made to simplify the governing mass and momentum conservation equations. It should be noted that the flow domain is restricted to the region inside the rotating cone. To describe this system, spherical coordinates in three dimensions (r, θ and ϕ) are appropriate where in addition the time coordinate (t) is required to study transient effects. The origin of the spherical coordinate system is situated at the virtual tip of the cone. Therefore, the spherical coordinates have the following ranges:

$$\mathrm{r_i} \leq \mathrm{r} \leq \mathrm{r_o} \wedge 0 \leq \theta \leq \theta_\mathrm{w} \wedge 0 \leq \phi \leq 2\pi \tag{A1}$$

as indicated in Figure 1.

In this study it will be assumed that the liquid flow in the rotating cone is symmetrical in the direction of rotation and therefore all quantities describing the flow are independent of the ϕ-coordinate:

$$\frac{\partial}{\partial \phi}\,(\ldots) = 0 \tag{A2}$$

The bulk gas is treated as a void, having no properties except that it takes up the space left by the fluid and it possesses an atmospheric pressure. The characteristic quantities of the single fluid are the r-, θ- and ϕ-components of the velocity vector and the internal pressure.

The location of the free surface between the fluid and the void is marked and traced according to the VOF method. Regarding the internal viscous stresses, the single fluid is assumed to behave like a Newtonian fluid with a constant density.

Finally, the gravitational force acting on the fluid is expressed by the components of the governing gravitational constant:

$$g = (-g\cos\theta, g\sin\theta, 0) \tag{A3}$$

Model equations

When the assumptions mentioned above are applied to the mass and momentum conservation equations, their simplified versions specific to a single fluid flow in a rotating cone are obtained. They are presented below (Bird *et al.*, 1960).

Conservation of mass:

$$\rho\left(\frac{2v_r}{r} + \frac{\partial v_r}{\partial r} + \frac{\cot\theta v_\theta}{r} + \frac{1}{r}\frac{\partial v_\theta}{\partial\theta}\right) = 0 \tag{A4}$$

Momentum equation in r-direction:

$$\begin{aligned}\nu\left(\frac{\partial^2 v_r}{\partial r^2} + \frac{1}{r^2}\frac{\partial^2 v_r}{\partial\theta^2}\right) + \left(v_r - \frac{4\nu}{r}\right)\frac{\partial v_r}{\partial r} + \left(\frac{v_\theta}{r} - \frac{\nu\cot\theta}{r^2}\right)\frac{\partial v_r}{\partial\theta} - \frac{1}{\rho}\frac{\partial p}{\partial r} - \frac{v_\theta^2}{r} - \frac{v_\phi^2}{r} \\ - \frac{2\nu v_r}{r} + g\cos\theta = 0\end{aligned} \tag{A5}$$

Momentum equation in θ-direction:

$$\begin{aligned}-\nu\left(\frac{\partial^2 v_\theta}{\partial r^2} + \frac{1}{r^2}\frac{\partial^2 v_\theta}{\partial\theta^2}\right) + \left(v_r - \frac{2\nu}{r}\right)\frac{\partial v_\theta}{\partial r} + \left(\frac{v_\theta}{r} - \frac{\nu\left(\cot^2\theta + 1\right)}{r^2}\right)\frac{\partial v_\theta}{\partial\theta} \\ - \frac{2\nu}{r}\frac{\partial v_r}{\partial\theta} - \frac{1}{\rho r}\frac{\partial p}{\partial\theta} - \frac{v_r v_\theta}{r} - \frac{v_\phi^2\cot\theta}{r} - g\sin\theta = 0\end{aligned} \tag{A6}$$

Momentum equation in φ-direction:

$$\begin{aligned}-\nu\left(\frac{\partial^2 v_\phi}{\partial r^2} + \frac{1}{r^2}\frac{\partial^2 v_\phi}{\partial\theta^2}\right) + \left(v_r - \frac{2\nu}{r}\right)\frac{\partial v_\phi}{\partial r} \\ + \left(\frac{v_\theta}{r} - \frac{\nu\left(\cot^2\theta + 1\right)}{r^2}\right)\frac{\partial v_\phi}{\partial\theta} - \frac{v_r v_\phi}{r} - \frac{v_\phi v_\theta\cot\theta}{r} = 0\end{aligned} \tag{A7}$$

It is necessary to define and trace the Eulerian location of the free surface. In our study the VOF-method described by Hirt and Nichols (1981) was applied to deal with this complicated problem. Within the framework of the VOF-method the fractional amount of fluid F is invoked to track the interface in the computational domain as discussed extensively in this paper. The development of the free surface is propagated as a Lagrangian invariant described by the partial differential free surface equation:

$$\frac{DF}{Dt} = \frac{\partial F}{\partial t} + (\nabla\cdot Fv) = 0 \tag{A8}$$

Numerical treatment

The conservation equations for mass and momentum (equations (A4 to A7) are discretized according to the semi-implicit finite difference approximation for staggered fixed Eulerian grid cells. Subsequently, the fluid flow variables are computed iteratively via a pressure correction technique employing a whole field solution strategy (see Kuipers *et al.* (1992)).

The computation of the solution of the conservation equations starts with the initialization of the velocity fields to conform to the initial conditions. The components of the momentum conservation equation are iteratively solved according to the mass conservation equation to yield

an improved guess for the velocity fields. Ultimately, the velocity fields will converge to the solution of the conservation equations for the current time level. Finally, the boundary conditions are applied. The velocity fields of the previous time level are used as an initial guess and the algorithm is repeated until the velocity fields arrive at the steady-state solution.

The velocity fields resulting from the substitution of a guessed pressure field into the components of the momentum conservation equation will not satisfy the mass conservation equation, unless the guessed pressure field is correct. If the guessed pressure field is not correct, it is improved in such a way that the mass conservation equation will progressively get closer to being satisfied. This improvement is accomplished by computing a pressure correction. This pressure correction is determined by the way the mass conservation equation responds to the guessed velocity fields that again respond to the guessed pressure field. Thus, the pressure field is used as a driving force to converge the velocity fields to the solution of the conservation equations.

Since the free surface boundary pressure conditions depend on the pressure of adjacent interpolation cells, these boundary conditions also have to be incorporated in the pressure field computation. The flow variables are not defined for empty cells; thus the velocity and pressure fields do not have to be calculated for these cells.

In short, the computation scheme shown in Figure A1 is applied to compute the dependent flow variables, according to the initial and boundary conditions, for each time interval until steady-state convergence.

First of all, the dependent flow variables are initialized to conform to the initial conditions. A pressure field is guessed and the guessed velocity fields are computed from the components of the momentum equations. The internal fluid mass conservation and free surface pressure defects (i.e. the deviation from mass conservation) are computed from the mass conservation equation and the free surface pressure equation respectively.

If the defects do not equal zero, the pressure corrections are computed according to the magnitude and dependence of the defects on the guessed pressure field. An improved pressure field is computed by adding the pressure corrections to the guessed pressure field and the algorithm is repeated.

If the defects equal zero, the ϕ-coordinate velocity is computed and the new location of the free surface boundary is computed from the velocity and pressure fields. Finally, the free surface velocity boundary conditions are applied and the velocity, pressure and fraction of volume fields are stored.

After each time iteration, the convergence criterion applied to the newly computed flow variables is checked. If the flow variables have not reached their steady state, the computation is repeated for the next time level; otherwise the computation is aborted. The computation scheme is presented in Figure A1 (overleaf).

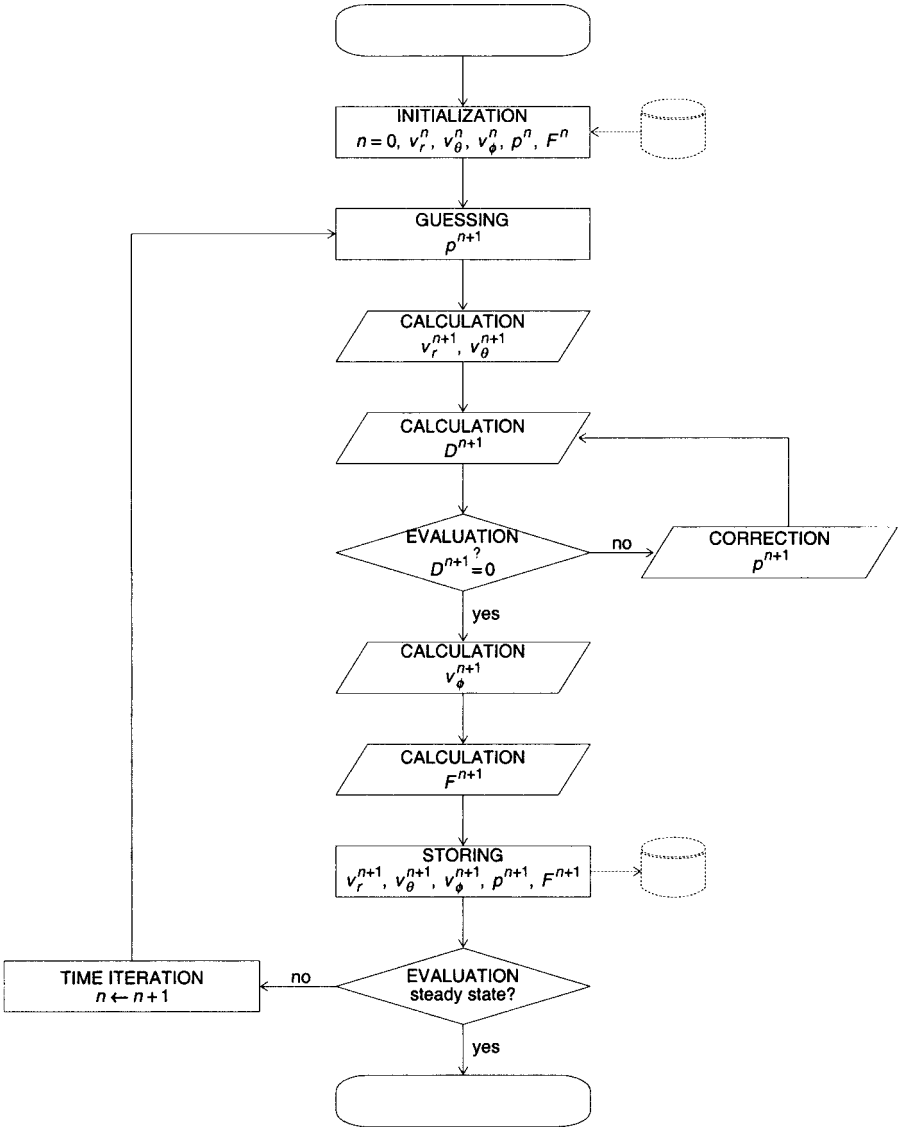

Figure A1.
Computation scheme